Journal of Materials Chemistry A

Accepted Manuscript

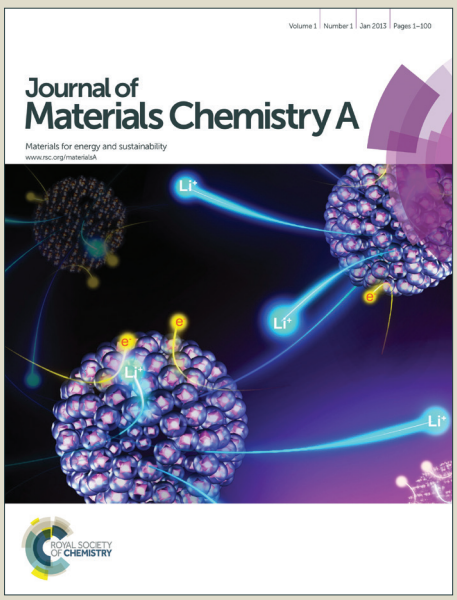

ROYAL SOCIETY OF CHEMISTRY

www.rsc.org/materialsA

Theoretical insight into the roles of cocatalysts in Ni-NiO/β-Ga_2O_3 photocatalyst for overall water splitting

Taifeng Liu,[ab] Ionut Tranca,[c] Jingxiu Yang,[ab] Xin Zhou[a]* and Can Li[a]*

a State Key Laboratory of Catalysis, Dalian Institute of Chemical Physics, Chinese Academy of Sciences, Dalian National Laboratory for Clean Energy, Dalian 116023, China. E-mail: xzhou@dicp.ac.cn, canli@dicp.ac.cn

b Graduate University of Chinese Academy of Sciences, Beijing 100049, China

c Schuit Institute of Catalysis, Laboratory of Inorganic Materials Chemistry, Eindhoven University of Technology, Den Dolech 2, 5612 AZ Eindhoven, The Netherlands

Abstract

The formation and stability of Ni_n and $(NiO)_n$ (n=1-4) clusters on the β-Ga_2O_3 surface have been studied by means of first-principles density functional theory calculations. It is found that the optimum interaction of the Ni_n and $(NiO)_n$ clusters with the surface requires different surface sites. This optimizes the formation of interfacial bonds between the atoms from clusters and the coordinatively unsaturated atoms from the surface. The stability of the adsorbed Ni clusters increases with the number of Ni atoms. In Ni_n/Ga_2O_3 system, as the Ga unoccupied states overlap with the unoccupied Ni state, the excited electrons transferred from Ga to Ni participate in proton reduction reaction. Our calculations show that $(NiO)_n$ clusters strongly adsorb on the Ga_2O_3 surface due to the negative adsorption energies within -1.9 eV ~ -3.7 eV. For $(NiO)_n/Ga_2O_3$, occupied states from the $(NiO)_n$ cluster may accept the holes from O atoms in Ga_2O_3 surface to take part in photocatalytic water oxidation reaction.

1. Introduction

Photocatalytic overall splitting of water over semiconductors has drawn great attention as one of possible strategies for environmental remediation and energy conversion.[1-5] Generally, a heterogeneous photocatalyst system is composed of semiconductor and cocatalysts.[6] The semiconductor is responsible for harvesting light, while photocatalytic reactions take place on cocatalysts loaded on the semiconductor. Cocatalysts can not only serve as reaction sites and catalyze reactions, but also promote the charge separation and transport driven by junctions/interfaces formed between cocatalyst and light harvesting semiconductor.[7] Many researches show that loading suitable cocatalysts can significantly increase the photocatalytic activities of hydrogen and oxygen evolution reactions.[8-12] Typically, the cocatalyst is a noble metal for reduction reactions (such as Pt, Pd, Ru, Rh and Au) or transition-metal oxide for oxidation reactions (such as CoO_x, NiO_x, IrO_2, MnO_x and RuO_2).

Nickel oxide has often been employed in many photocatalytic systems for water splitting,[3] such as Ga_2O_3,[13,14] $SrTiO_3$,[15-17] La: $KTaO_3$,[18] $K_4Nb_6O_{17}$,[19] and $Ba_5Nb_4O_{15}$.[20] In general, the pretreatment of H_2 reduction and subsequent O_2 oxidation is indispensable for the nickel oxide loaded photocatalysts to show high activities. So the pretreated nickel oxide cocatalyst is often denoted as NiO_x in literatures.[13-20] Ga_2O_3, as a representative of semiconductors with a d^{10} electronic configuration, exhibits high photocatalytic activity for water splitting.[13,14] The results reported by Yanagida *et al.* show that only H_2 production was observed when Ga_2O_3 was used as the photocatalyst without NiO_x loading, and the activity was relatively low.[13] A recent

work showed that NiO_x loading is necessary to induce the stoichiometric formation of H_2 and O_2 by photocatalytic decomposition of water on Ga_2O_3 with tunable α-β phase junctions.[14]

Cocatalysts are typically present as nanoparticles on the semiconductor surface loaded by impregnation or *in situ* photo-deposition.[21] The structural complexity of the nano-sized metal or metal oxide clusters on semiconductor surfaces makes it difficult to obtain structural and electronic information for these systems even under well-defined experimental conditions. Theoretical studies based on first-principles electronic structure calculations have proven to be useful for complementing the experimental results to illuminate the relationship between the surface structure and the physical and chemical properties of semiconductors, and further to understand the mechanism of photocatalytic reaction.[22-30]

Although experimental observations indicate that cocatalysts play an important role in promoting charge separation and increasing activity in photocatalytic systems, several critical questions on cocatalysts are still open. For example, how and where does a cocatalyst locate on the surface of semiconductors? How does the adsorption of cocatalyst affect the electronic properties of photocatalysts? Why does loading cocatalysts promote the charge separation? To answer these questions, we took Ni-NiO/β-Ga_2O_3 photocatalytic system as a model and performed detailed theoretical calculations. In the present work, we computed the surface structures and formation energies of five different surfaces of β-Ga_2O_3, determined the stable configurations of Ni_n and $(NiO)_n$ (n=1-4) clusters adsorbed on the most stable surface of β-Ga_2O_3, and

investigated the electronic properties and charge distribution for these systems. We found that small Ni_n and $(NiO)_n$ clusters tend to form on different sites of the surface. The electronic structure analyses indicate that Ni_n/Ga_2O_3 systems participate in photocatalytic hydrogen evolution reaction (HER) while $(NiO)_n/Ga_2O_3$ systems tend to take part in photocatalyitc oxygen evolution reaction (OER).

2. Computational Details

All the DFT spin-polarized calculations were performed with the VASP (Vienna Ab initio Simulation Package) code.[31,32] The exchange correlation potential was described through the Perdew-Burke-Ernzerhof (PBE) functional within the generalized gradient approximation formalism.[33] The projector-augmented wave method was applied to describe electron-ion interactions.[34,35] A Hubbard *U* term acting on the Ni 3d orbitals was added to the standard PBE functional employing the rotationally invariant formalism developed by Dudarev et al.,[36] in which only the difference (U_{eff} = *U* - *J*) between the Coulomb *U* and exchange *J* parameters is considered. In the present work, a value of U_{eff}=5.3 eV was used, which was calculated self-consistently by Ferrari *et al*.[37] and which is in the range of 5-6 eV interval found in the literature.[36,38,39]

Among the five different crystalline structures of Ga_2O_3, β-Ga_2O_3 is the most stable crystal phase.[40] This crystal phase exhibits excellent photocatalytic activity,[41,42] and it is the subject of extensive experimental and theoretical studies.[43-49] So in this work, we chose β-Ga_2O_3 to represent the semiconductor in photocatalytic systems. Full optimization of the cell parameters for the bulk β-Ga_2O_3 with monoclinic structure

(Figure 1a) was carried out by using the 3×11×7 Monkhorst-Pack type *k*-point sampling. The cutoff energy for the plane wave basis set was fixed at 520 eV. The calculated lattice parameters, *a*=12.504 Å, *b*=3.101 Å, *c*=5.915 Å, and β=103.71°, are in good agreement with the experimental data.[50] For all the surface calculations a vacuum layer of 15 Å was used in order to avoid the interaction between periodic slabs. For the calculation of the surface energy, (1×1) cells were considered, a Monkhorst-Pack set of 3×3×1 *k*-points was applied and all the atomic layers in the slabs were allowed to relax. During the optimization of the surfaces covered with adsorbates, a (3×2) supercell including a cell composition $(Ga_2O_3)_{24}$ was used. The upper half of the slab and the adsorbates were allowed to relax, while the bottom half of the slab was fixed at its optimized bulk position. Dipolar corrections were included along the axis normal to the surface. The geometries were considered to be converged when the forces on each ion were less than 0.01 eV/Å.

On top of the optimized geometries obtained at the GGA-PBE level, a more accurate approach, the hybrid HSE06 functional,[51-53] was used to calculate the electronic properties for the most stable structures. This is necessary in order to achieve a good agreement between the experimental and the theoretical band gaps. The HSE06 functional includes a fraction α, of screened, short-range HF exchange to improve the derivative discontinuity of the Kohn-Sham potential for integer electron numbers. The percentage of HF exchange in a hybrid functional is not a universal constant and the optimal value can be system-dependent. The band gap of bulk β-Ga_2O_3 was obtained from experiments to be in the range of 4.2-4.7 eV. [14,33,54,55] In

the present work, an α=0.3 was used as this value can yield a good agreement between the computed band gap (4.5 eV) and the experimental results.

3. Results and Discussion

3.1. Bulk and surface properties

Figure 1a shows that the unit cell of β-Ga_2O_3 contains four Ga_2O_3 formula units with two nonequivalent Ga sites and three nonequivalent O sites. Ga(I) is bonded to four O anions in the form of a distorted tetrahedron, while Ga(II) forms a highly distorted octahedron with six O anions. Each O(I) is threefold coordinated and shared by two octahedra and one tetrahedron. Each O(II) is also threefold coordinated and lies at the intersection of two tetrahedra and one octahedron. Each O(III) is fourfold coordinated and connected with three octahedra and one tetrahedron. The computed bond lengths are as follows: Ga(I)-O(I)=1.864 Å, Ga(I)-O(II)=1.867 Å, Ga(I)-O(III)= 1.894 Å, Ga(II)-O(I)=1.969 Å, Ga(II)-O(II)=1.951 Å, Ga(II)-O(III)= 2.073 Å. All are in good agreement with the experimental values.[50]

Five β-Ga_2O_3 surfaces of interest are created by cleaving the optimized bulk structure through the corresponding planes, and the resultant structures are depicted in Figure 1b-f. They are denoted as (100)-A, (100)-B, (001)-A, (001)-B and (010), respectively. Structural differences for these surfaces were intensively investigated by Bermudez.[56] In order to estimate the relative stability of these surfaces, slabs with different numbers of stoichiometric repeated layers were constructed for each surface. The computed total energies of the slabs, together with their corresponding numbers of Ga_2O_3 units, were then fitted into the following equation to calculate the surface

formation energy γ,

$$\gamma = (E_{slab} - nE_{Ga_2O_3})/2A \quad (1)$$

where E_{slab} is the total energy of the slab, n is the number of Ga_2O_3 units in the slab, and $2A$ is the total exposed area of the two identical sides of the slab.

As shown in Figure 2, calculated surface energies are converged within 0.01-0.03 J/m^2 for (100), (001) and (010) when n reaches 4, 8, and 10, respectively. The computed value of surface energy is 0.84 J/m^2 for (100)-A, 0.47 J/m^2 for (100)-B, 1.75 J/m^2 for (001)-A, 1.18 J/m^2 for (001)-B and 1.49 J/m^2 for (010). Our results show that the (100)-B surface is the most stable one among the five surfaces we considered, which is in good agreement with available experimental and theoretical data.[56-58] Therefore, we focus our calculations and discussions on the (100)-B surface in the following parts.

As shown in Figure 1(c), the (100)-B surface is terminated by fivefold coordinated Ga(II) (Ga_{5c}(II)) and threefold coordinated O(III) (O_{3c}(III)). Ga(I) and O(I) atoms at the surface are fully coordinated, and there are no O(II) atoms in the surface plane. The side view of this surface is like a wave. The quadrilaterals composed of Ga_{5c}(II), O_{3c}(III) and O(I) atoms are located in wave crest, while Ga(I) atoms are situated in wave trough. Based on the relaxed surface structure of (100)-B, total density of states (TDOS) and partial density of states (PDOS) have been evaluated by means of HSE06. As shown in Figure 3, the valence band maximum (VBM) is mainly composed of O 2p states, slightly hybridized with Ga 3d and 4p states. Ga 4s states contribute more to the lower valence bands. The conduction band minimum (CBM) consists mostly of

Ga 4s states. The valence bands exhibits the characteristic of mixed O 2p, Ga 4s, 4p and 3d states. The strong mixing of O and Ga orbitals is indicative of the high degree of covalent bonding in this semiconductor. The value of band gap is computed to be 4.0 eV, which is smaller than that of the bulk (4.5 eV) due to the surface dangling bonds.

3.2. Formation of Ni_n clusters on (100)-B surface of β-Ga_2O_3

To obtain the most stable structure for a given Ni_n (n=1-4) cluster supported on Ga_2O_3(100), the cluster was placed on the surface in all possible positions and in different orientations. The four most stable configurations for each Ni_n/Ga_2O_3(100) are shown in Figure 4, while the other configurations are summarized in the supplementary material (see Figure S1). Relative energies with respect to the corresponding lowest-energy structures are shown in the figures. All of the obtained configurations show that after adding Ni_n clusters onto the surface, there are bonds formed between the cluster and surface, which are defined as "interfacial bonds" in this work. This means that the interaction between clusters and Ga_2O_3 surface belongs to the chemical adsorption. The adsorption energy, E_{ads}, of a cluster adsorbed on the β-Ga_2O_3 surface was defined as:

$$E_{ads} = E_{total} - E_{surface} - E_{cluster} \qquad (2)$$

where E_{total} is the total energy of the Ga_2O_3 surface with a cluster, $E_{surface}$ is the total energy of the bare and relaxed surface, and $E_{cluster}$ is the energy of optimized cluster in the gas phase. To better understand the nucleation or growth of Ni_n clusters on the support, the average binding energy $E_{binding}$ of Ni_n cluster adsorbed on the β-Ga_2O_3

surface was calculated as

$$E_{binding} = (E_{total} - E_{surface} - nE_{Ni})/n \qquad (3)$$

where E_{Ni} is the energy carried by a free Ni atom in vacuum.

The key structural parameters for the most stable configuration of each $Ni_n/Ga_2O_3(100)$ ensemble are displayed in Figure 5. As shown in Figure 5(a), the most stable adsorption site for an isolated Ni atom is in the middle of two nearest O_{3c}(III) atoms with an adsorption energy of -2.16 eV, resulting in two Ni-O bonds with an equal bond length of 1.856 Å, and the distance of Ga_{5c}(II) and Ni atom to be 2.289 Å. The adsorption of Ni atom increases the distance between O_{3c}(III) atom and Ga_{5c}(II) atom by about 0.58 Å compared with the value for a clean surface. The adsorption of the Ni monomer induces therefore significant surface modifications. We have tested the adsorption of a single Ni atom on top of a single O(III) or O(I) atom. In the optimized structure, the Ni atom migrated to the bridge position, which is the same as the most stable structure. This means that the Ni atom prefers a bridge adsorption between two oxygens instead of a top one on the surface oxygen atom. Comparing the relative energies of all Ni_1/Ga_2O_3 optimized configurations from Figure 4, one can notice that the formation of interfacial bonds between the Ni atom and the coordinatively saturated gallium/oxygen atoms from the surface leads to less stable structures. Only the structure with the Ni binding to the O(III) and Ga(II) is stable, as it brings the three surface atoms to a coordination number similar to that in bulk Ga_2O_3.

When Ni_2 dimer is adsorbed on the $Ga_2O_3(100)$ surface, the most energetically

favorable configuration is the horizontal adsorption (see Figure 4), with an adsorption energy of -2.47 eV. The two Ni atoms are symmetrically located on the surface, forming six interfacial bonds. Owing to the adsorption of the additional Ni atom, the already bonded Ni atom is lifted and the bond length of Ni-O is computed to be 2.032 Å (+0.18 Å compared with the Ni-O bond from $Ni/Ga_2O_3(100)$). Similarly, the Ga-Ni bond is also lengthened by 0.25 Å. The calculated distance between the two Ni atoms is 2.429 Å, which is longer than that within Ni_2 cluster in gas phase by 0.065 Å. As shown in Figure S1, like in the case of Ni monomer, more bonds formation between Ni_2 cluster and the fully saturated Ga and O atoms from the surface lead to less favorable structures. The average binding energy of the most stable structure is calculated to be -2.20 eV, which suggests that the addition of the second Ni atom slightly improves the stability of the first Ni atom.

There are two stable configurations for the isolated Ni_3 ternary cluster: the regular triangular form and the beeline form, and the latter is calculated to be more stable than the former by 0.12 eV. These two initial structures of Ni_3 cluster were attached to the surface in different directions and positions. After optimization, some original linear configurations are curled (see structures i and k in Figure S1). Our calculations show that the total energy of the triangular configurations is always lower than that of the linear ones. For the lowest-energy structure (see Figure 4 and Figure 5(c)), one Ni atom is located in the most stable adsorption site for single Ni atom attached to the surface, and the other two Ni atoms symmetrically form bonds with O(I) atoms. The Ni-O(III)/O(I) and Ni-Ni bonds are predicted to be 2.122 Å/2.008 Å and 2.336-2.400

Å, respectively. The Ni-Ni bonds within the triangular form are shorter and stronger than in the adsorbed dimer. Corroborating this with the larger average binding energy for Ni_3 cluster on the surface (-2.28 eV), it suggests that the formation of the Ni_3 cluster is favorable on the surface.

The initial adsorption configurations for the Ni_4 cluster were set to be tetrahedral and rhombic. The tetrahedral structure is computed to be energetically more favorable than the rhombic one by 0.10 eV in gas phase. Ten stable adsorption configurations were obtained after optimizations, as displayed in Figure 4 and S1. The results show that the adsorption of the tetrahedral Ni_4 cluster is energetically more favorable than that of the rhombic one. As shown in Figure 5(d), the most stable configuration is generated by adding an extra Ni atom above the plane of the Ni_3 cluster in the lowest-energy structure of $Ni_3/Ga_2O_3(100)$. The introduction of the extra Ni atom decreases the average binding energy to -2.34 eV, and further improves the stability of Ni_n cluster on β-Ga_2O_3 surface. The Ni-O(I)/O(III) and Ni-Ga bonds are calculated to be 1.95 Å/2.085 Å and 2.707 Å, respectively. The Ni-Ni bonds are in the range of 2.409~2.455 Å.

Our calculated results show that the addition of a new Ni atom to an existing Ni_n cluster adsorbed on the $Ga_2O_3(100)$ surface is energetically favorable. If the Ni_n cluster binds to coordinatively saturated Ga(I) atoms from the surface, the adsorption structure is energetically unfavorable. The average binding energy gradually decreases with the increase of *n* value in Ni_n cluster, which indicates a tendency for this metal to aggregate on the surface. The most stable configuration of every Ni_n cluster (n=1-4)

indicates that one Ni cluster tends to form above Ga(I) atoms and between O(I) and O_{3c}(III) atoms.

To investigate the charge rearrangement upon the formed interface between the Ga_2O_3 surface and Ni_n cluster, Bader charge analyses has been performed.[59-60] The optimized geometries of the surface with adsorbed cluster, clean surface, and isolated cluster are kept fixed for the Bader charge analyses. The results shown in Table 1 demonstrate that when a Ni_n cluster is adsorbed onto the β-Ga_2O_3(100) surface, it will lose electrons and carry some positive charge. It is interesting to note that for the three-dimensional Ni_4 cluster adsorbed system, only the Ni atoms bonded to the surface donate electrons to the surface, while the Ni atom at the top of the tetrahedron is nearly neutral, which indicates that at low metal coverage, the nickel adatom is ionic because it is directly bonded to surface oxygen; with the increase of the coverage, the newly arrived nickel adatoms are neutral unless they are bonded to the surface atoms.

In order to understand the effect of adsorbing the metal cluster on the electronic structure of the substrate, we have calculated the total density of states (TDOS) and projected density of states (PDOS) for Ni 3d states for the lowest-energy configurations of Ni_n/Ga_2O_3(100). As shown in Figure 6, for the Ni_n/Ga_2O_3 (n=1,3 and 4) system, there is an unoccupied Ni state about 2 eV above the Fermi level. As shown in Figure 3, the CBM of Ga_2O_3 surface is mainly composed of Ga 4s orbitals. So the empty Ni state overlaps with the empty Ga states. Upon the photoexcitation, electrons removed from the O occupied states move to the Ga unoccupied states. As

the Ga unoccupied states overlap with the unoccupied Ni state, the electron can transfer from Ga to Ni. Consequently, the accumulating electrons on the Ni_n cluster may participate in proton reduction for HER. From Figure 6, one can also find that remarkable occupied states of Ni appear in VBM of system. During the photocatalytic reaction, an electron can be excited from an O atom to an unoccupied Ga atom. This results in the formation of a hole on the O atom. The hole can be moved from the O atom to the Ni atom in Ni_n cluster. So in principle Ni atoms can also contribute to the OER. However, using the Ni metal for OER is not really appropriate because it will probably lead to NiO.

3.3. Formation of $(NiO)_n$ clusters on (100)-B surface of β-Ga_2O_3

For $(NiO)_n/Ga_2O_3(100)$, the most stable energy structures obtained from our calculations are plotted in Figure 7, and other less stable structures are shown in Figure S2. For every composition, key structural parameters of the lowest-energy configurations are summarized in Figure 8. The adsorption energy for clusters is calculated based on Equation (2), and the obtained results are shown in Table 1. Negative adsorption energy means that the adsorbed structure is stable.

For $NiO/Ga_2O_3(100)$ system, the most stable structure for this composition is obtained by introducing an additive oxygen atom to the most stable structure of Ni/Ga_2O_3. As shown in Figure 8(a), the O atom binds to the surface Ga_{5c} atom through a bond length of 1.885 Å. Due to the adsorption of the O atom, the bonded Ni atom is lifted and the bond length of $Ni\text{-}O_{3c}$ is lengthened by 0.18 Å compared with that of single Ni atom adsorbed on the surface. The Ni-O bond is computed to be

1.776 Å. The adsorption energy of NiO cluster is calculated to be -1.92 eV, indicating the stability of this configuration.

For the case of $(NiO)_2/Ga_2O_3(100)$, seven structures are obtained as shown in Figure 7 and Figure S2. The lowest-energy configuration consists of a -Ni-O-Ni-O- four-membered ring adsorbed above the rhombic fragment of -O-Ga-O-Ga- with the formation of four interfacial bonds. As can be seen from Figure 8(b), the bond lengths of Ga-O, Ni-O(III) and Ni-O(I) are computed to be 2.000 Å, 1.940 Å and 1.935 Å, respectively. The average distance of the Ni-O bonds within the cluster is of 1.886 Å, which is larger by 0.11 Å than that in the NiO monomer supported on the $Ga_2O_3(100)$ surface. The adsorption energy of this structure is predicted to be -3.67 eV, which is lower than that of NiO adsorption by 1.65 eV. Examining the relative energy of different structures from Figure 7 and Figure S2, one can find that the structure with Ni_2O_2 located above Ga(I) atoms as well as between O(I) and O_{3c}(III) atoms is less stable than the one with Ni_2O_2 situated above the rhombic fragment of -O-Ga-O-Ga-.

When a $(NiO)_3$ cluster was attached to the surface, both three-dimensional and two-dimensional models were considered. The most stable structure is a two-dimensional planar six-member ring structure located atop of the rhombic fragment of -O-Ga-O-Ga-, and with the adsorption energy of -2.57 eV. As shown in Figure 8(c), the three Ni atoms are coordinated to surface oxygen atoms with Ni-O bonds of 2.012, 2.45 and 2.039 Å, respectively. Two oxygen atoms from the cluster bind to Ga atoms from the surface and have Ga-O distances of 1.961 and 1.982 Å, respectively. The third oxygen from cluster does not connect to any Ga atom. The calculated Ni-O bond

lengths in cluster are in the range of 1.797~1.910 Å.

For the Ni_4O_4 cluster adsorbed on the $Ga_2O_3(100)$ surface, several initial configurations have been optimized. For the most stable structure **a**, shown in Figure 7 and in Figure 8(d), the adsorbed cluster is symmetrically bonded to the surface by four Ni-O and two Ga-O bonds. Two Ni atoms bond to two O(I) with equal distances of 1.938 Å, while the other two Ni atoms bond to two O(III) with equal distances of 1.937 Å. Two oxygen atoms from the cluster make bonds with 5-fold coordinated Ga atoms from the surface, with Ga-O distances of 2.038 Å and 2.042 Å. The other two oxygen atoms from the cluster bind only internally in the cluster, and have no connection to the surface. The eight-member ring of Ni_4O_4 cluster is made up from two kinds of Ni-O bonds with distances of 1.764 and 1.870 Å, respectively. The second most stable structure **b**, displayed in Figure 7, shows a rectangle cluster composed of three -Ni-O- four-member rings parallel adsorbed on the surface, which is less stable by 0.18 eV than the lowest-energy structure. The third most stable structure **c** exhibits a cubic Ni_4O_4 cluster connected to the surface Ga and O atoms and located in the same site of surface as Ni_2O_2 cluster. Compared with the most stable structure, this configuration is energetically less favorable by 0.45 eV. In the gas phase, the rectangle Ni_4O_4 cluster in structure **b** is calculated to be the most stable, which is lower than the cluster in structure **a** and the cubic cluster in structure **c** by 0.04 eV and 0.87 eV, respectively. The adsorption energies computed for the Ni_4O_4 clusters on the surface are of -2.96 eV for the most stable configuration **a**, -2.74 eV for structure **b**, and -3.35 eV for structure **c**. These results suggest that the cubic Ni_4O_4

cluster adsorbs stronger on the Ga_2O_3 surface than the planar structures.

As indicated from the calculations above, $(NiO)_n$ clusters tend to maximize interfacial bonds with coordinatively unsaturated Ga and O atoms of $Ga_2O_3(100)$ surface. The calculated adsorption energies of low-energy structures indicate that there are strong interactions between nickel oxide nanoclusters and surface. Unlike Ni_n clusters, $(NiO)_n$ clusters prefer to be formed above the rhombic fragment composed of Ga_{5c}(III), O(I) and O_{3c}(III) atoms. In other words, small Ni_n and $(NiO)_n$ clusters will tend to form on different sites of the surface.

The charge distribution at the interface between the $(NiO)_n$ clusters and the surface has been examined through the use of the Bader charge analysis. As shown in Table 1, after attaching to the surface, the Ni atoms from the $(NiO)_n$ clusters show positive charge while the O negative charge. This indicates that the charge flow occurs from Ni atoms to surface O atoms, and from surface Ga atoms to cluster O atoms simultaneously. The number of electrons received by O in $(NiO)_n$ clusters is slightly smaller than the number of electrons given away by Ni. As a result, the total charge on the $(NiO)_n$ cluster is slightly positive. With the increase of the cluster size, the amount of the charge transferred between the surface and the cluster increases significantly due to the larger number of bonds formed between the surface and the cluster.

More insight into the adsorption effects of the $(NiO)_n$ clusters can be obtained from the analysis of the electronic density of states. In Figure 9 we present the calculated HSE06 TDOS and PDOS for Ni 3d states and O 2p states for every $(NiO)_n$ cluster in the most stable adsorbed configuration. The strong mixing of O and Ni states is

indicative for the covalent bonding in NiO. Some of mixed states are located in VBM and others are at and below the Fermi level. Upon light irradiation, the electrons in the VBM of Ga_2O_3 are excited to the CBM, while the holes are left in the VBM. Since the occupied states from the $(NiO)_n$ cluster are higher in energy than the VBM, the electrons in $(NiO)_n$ tend to transfer to the VBM of Ga_2O_3. And then the holes generated in $(NiO)_n$ clusters will participate in the photocatalytic OER. As shown in Figure 9, one can find that some Ni unoccupied states are located ~ 4.5 eV above the Fermi level. The high position of the Ni unoccupied states will make the HER unfavorable.

Conclusions

In this work, we have performed a systematic DFT study on the relative stabilities of the low-index surfaces of β-Ga_2O_3, and on the stable adsorption sites for Ni_n and $(NiO)_n$ clusters supported on the surface. It was found that small Ni_n clusters tend to be formed above Ga(I) atoms and between O(I) and O_{3c}(III) atoms, while $(NiO)_n$ clusters tend to grow on the rhombic fragment composed of Ga_{5c}(III), O(I) and O_{3c}(III) atoms. For Ni_n/Ga_2O_3 systems, the binding energy decreases with the increment of Ni coverage (from Ni_1 to Ni_4), which indicates that larger clusters are energetically more stable than smaller ones. $(NiO)_n$ clusters are calculated to strongly adsorb on the Ga_2O_3 surface due to the negative adsorption energies within -1.9 eV~ -3.7 eV.

The electronic structure analyses indicate that for Ni_n/Ga_2O_3 systems, the unoccupied Ni states overlap with the Ga unoccupied states. Upon the irradiation of light, the excited electron can transfer from Ga to Ni. Consequently, the accumulating

electrons on Ni_n clusters may participate in photocatalytic HER. As to $(NiO)_n/Ga_2O_3$, occupied states from the $(NiO)_n$ cluster may accept the holes from O atoms in Ga_2O_3 surface to take part in photocatalytic OER. The determination of the stable structures and electronic structures for Ni_n, and $(NiO)_n$ adsorbed on the β-Ga_2O_3 surface provides a foundation for further investigations on the mechanism of photocatalytic water-splitting reaction in NiO_x/Ga_2O_3 system as well as other NiO_x/semiconductor systems.

Acknowledgements

This work is financially supported by National Natural Science Foundation of China under Grant 21473183 and 21361140346. We have also appreciated the financial support by the National Basic Research Program of China (973 program 2014CB239400).

References

1 S. Y. Reece, J. A. Hamel, K. Sung, T. D. Jarvi, A. J. Esswein, J. J. H. Pijpers and D. G. Nocera, *Science*, 2011, **334**, 645-648.

2 K. Maeda, K. Teramura, D. L. Lu, T. Takata, N. Saito, Y. Inoue and K. Domen, *Nature*, 2006, **440**, 295-295.

3 A. Kudo and Y. Miseki, *Chem. Soc. Rev.* 2009, **38**, 253-278.

4 X. Chen, S. Shen, L. Guo and S. S. Mao, *Chem. Rev.* 2010, **110**, 6503-6570.

5 A. Fujishima and K. Honda, *Nature*, 1972, **238**, 37-38.

6 J. Yang, D. Wang, H. Han and C. Li, *Acc. Chem. Res.*, 2013, **46**, 1900-1909.

7 X. Zong, H. J. Yan, G. P. Wu, G. J. Ma, F. Y. Wen, L. Wang and C. Li, *J. Am. Chem. Soc.*, 2008,

130, 7176-7177.

8 H. Yan, J. Yang, G. Ma, G. Wu, X. Zong, Z. Lei, J. Shi and C. Li, *J. Catal.*, 2009, **266**, 165-168.

9 D. Y. C. Leung, X. L. Fu, C. F. Wang, M. Ni, M. K. H. Leung, X. X. Wang and X. Z. Fu, *ChemSusChem,* 2010, **3**, 681-694.

10 D. Wang, R. Li, J. Zhu, J. Shi, J. Han, X. Zong and C. Li, *J. Phys. Chem. C*, 2012, **116**, 5082-5089.

11 K. S. S. Ma, K. Maeda, R. Abe and K. Domen, *Energy Environ. Sci.*, 2012, **5**, 8390-8397.

12 M. Higashi, K. Domen and R. Abe, *J. Am. Chem. Soc.*, 2012, **134**, 6968-6971.

13 T. Yanagida, Y. Sakata and H. Imamura, *Chem. Lett.*, 2004, **33**, 726-727.

14 X. Wang, Q. Xu, M. Li, S. Shen, X. Wang, Y. Wang, Z. Feng, J. Shi, H. Han and C. Li, *Angew.Chem. Int. Ed.* 2012, **51**, 13089-13092.

15 K. Domen, A. Kudo and T. Onishi, *J. Catal.*, 1986, **102**, 92-98.

16 K. Sayama and H. Arakawa, *J. Photochem. Photobiol., A*, 1994, **77**, 243-247.

17 T. K. Townsend, N. D. Browning and F. E. Osterloh, *Energy Environ. Sci.*, 2012, **5**, 9543-9550.

18 H. Kato, K. Asakura and A. Kudo, *J. Am. Chem. Soc.*, 2003, **125**, 3082-3089.

19 A. Kudo, K. Sayama, A. Tanaka, K. Asakura, K. Domen, K. Maruya and T. Onishi, *J. Catal.*, 1989, **120**, 337-352.

20 Y. Miseki, H. Kato and A. Kudo, *Chem. Lett.*, 2006, **35**, 1052-1053.

21 K. Maeda, K. Teramura, D. Lu, N. Saito, Y. Inoue and K. Domen *Angew. Chem. Int. Ed.* 2006, **45**, 7806-7809.

22 D. Matthey, J. G. Wang, S. Wendt, J. Matthiesen, R. Schaub, E. Laegsgaard, B. Hammer and F. Besenbacher, *Science*, 2007, **315**, 1692-1696.

23 H. G. Yang, C. H. Sun, S. Z. Qiao, J. Zou, G. Liu, S. C. Smith, H. M. Cheng and G. Q. Lu, *Nature*, 2008, **453**, 638-641.

24 Y.-F. Li, Z.-P. Liu, L. L. Liu and W. Gao, *J. Am. Chem. Soc.*, 2010, **132**, 13008- 13015.

25 M. Setvin, U. Aschauer, P. Scheiber, Y.-F. Li, W. Hou, M. Schmid, A. Selloni and U. Diebold, *Science*, 2013, **341**, 988-991.

26 M. Zhang, J. Chen, Y. Yu and Y. Zhang, *Appl. Surf. Sci.*, 2013, **287**, 97-107.

27 C. D. Valentin, L. Giordano, G. Pacchioni and N. Rösch, *Surf. Sci.*, 2003, 522, 175-184.

28 E. Escamilla-Roa, V. Timon, A. Hernandez-Laguna, *Comput. Theo. Chem.*, 2012, **981**, 59-67.

29 Y. Pan, C. Liu, Q. Ge, *J. Catal.*, 2010, **272**, 227-234.

30 J. Li, E. Croiset, L. Ricardez-Sandoval, *J. Phys. Chem. C*, 2013, 117, 16907-16920.

31 G. Kresse and J.Furthmüller, *Phys. Rev. B,* 1996, **54**, 11169.

32 G. Kresse and J.Furthmüller, *Comput. Mater. Sci.*, 1996, **6**, 15-50.

33 J. P. Perdew, K. Burke and M.Ernzerhof, *Phys. Rev. Lett.*, 1996, **77**, 3865-3868.

34 P. E. Blochl, *Phys. Rev. B,* 1994, **50**, 17953-17979.

35 G. Kresse and J. Joubert, *Phys. Rev. B*, 1999, **59**, 1758-1775.

36 S. L. Dudarev, G. A. Botton, S. Y. Savrasov, C. J. Humphreys and A. P. Sutton, *Phys. Rev. B*, 1998, **57**, 1505-1509.

37 A. M. Ferrari, C. Pisani, F. Cinquini, L. Giordano and G. Pacchioni, *J. Chem. Phys.*, 2007, **127**, 174711.

38 W. E. Pickett, S. C. Erwin and E. C. Ethridge, *Phys. Rev. B*, 1998, **58**, 1201-1209.

39 O. Bengone, M. Alouani, P. Blöchl and J. Hugel, *Phys. Rev. B*, 2000, **62**, 16392- 16401.

40 R. Roy, V. G. Hill and E. F. Osborn, *J. Am. Chem. Soc.*, 1952, **74**, 719-722.

41 B. Zheng, W. Hua, Y. Yue and Z. Gao, *J. Catal.*, 2005, **232**, 143-151.

42 Y. Hou, L. Wu, X. Wang, Z. Ding, Z. Li and X. Fu, *J. Catal.*, 2007, **250**, 12-18.

43 H. He, R. Orlando, M. A. Blanco, R. Pandey, E. Amzallag, I. Baraille and M. Rérat, *Phys. Rev. B*, 2006, **74**, 195123.

44 S. Yoshioka, H. Hayashi, A. Kuwabara, F. Oba, K. Matsunaga and I. Tanaka, *J. Phys.: Condens. Matter*, 2007, **19**, 346211.

45 Y. Sakata, Y. Matsuda, T. Yanagida, K. Hirata, H. Imamura and K. Teramura. *Catal. Lett.*, 2008, **125**, 22-26.

46 T. C. Lovejoy, E. N. Yitamben, N. Shamir, J. Morales, E. G. Villora, K. Shimamura, S. Zheng, F. S. Ohuchi and M. A. Olmstead, *Appl. Phys. Lett.*, 2009, **94**, 081906-1-3.

47 Y. Hou, J. Zhang, Z. Ding and L. Wu, *Powder Technol.*, 2010, **203**, 440-446.

48 Y. Sakata, Y. Matsuda, T. Nakagawa, R. Yasunaga, H. Imamura and K. Teramura, *ChemSusChem*, 2011, **4**, 181-184.

49 T. Oshima, K. Kaminaga, H. Mashiko, A. Mukai, K. Sasak, T. Masui, A. Kuramata, S.Yamakoshi, and A. Ohtomo., *Jpn. J. Appl. Phys.* 2013, **52**, 111102.

50 S. Geller, *J. Chem. Phys.,* 1960, **33**, 676.

51 J. Heyd, G. E. Scuseria and M. Ernzerhof, *J. Chem. Phys.*, 2003, **118**, 8207-8215.

52 J. Heyd, G. E. Scuseria and M. Ernzerhof, *J. Chem. Phys.*, 2004, **121**,1187-1192.

53 J. Heyd, G. E. Scuseria and M. Ernzerhof, *J. Chem. Phys.*, 2006, **124**, 219906.

54 H. H. Tippins, *Phys. Rev. A*, 1965, 140, A316-A319.

55 N. Ueda, H. Hosono, R. Waseda, H. Kawazoe, *Appl. Phys. Lett.*, 1997, 71, 933- 935.

56 V. M. Bermudez, *Chem. Phys.*, 2006, **323**, 193-203.

57 Y. Tomm, P. Reiche, D. Klimm and T. Fukuda, *J. Cryst. Growth*, 2000, **220**, 510-514.

58 E. G. Villora, Y. Murakami, T. Sugawara, T. Atou, M. Kikuchi, D. Shindo and T. Fukuda, *Mater. Res. Bull.*, 2002, **37**, 769-774.

59 R. F. W. Bader, *Chem. Rev.*, 1991, **91**, 893-928.

60 W. Tang, E. Sanville, G. Henkelman, *J. Phys: Condens. Matter*, 2009, **21**, 084204.

Table 1. The adsorption energy E_{ads} (eV), binding energy E_{nuc} (eV) and the change of the total bader charge for Ni_n or Ni_nO_n clusters (a.u.) in Ni_n/Ga_2O_3 or Ni_nO_n/Ga_2O_3 systems, respectively. Only the most stable configuration for each composition is listed.

Configuration	E_{ads}	$E_{binding}$	$Q_{cluster}$	Configuration	E_{ads}	Q_{Ni}	Q_O	$Q_{cluster}$
Ni	-2.16	-2.16	+0.58	NiO	-1.92	+0.35	-0.30	+0.05
Ni_2	-2.47	-2.20	+0.73	Ni_2O_2	-3.67	+0.45	-0.35	+0.10
Ni_3	-4.94	-2.28	+0.72	Ni_3O_3	-2.57	+1.74	-1.62	+0.12
Ni_4	-6.83	-2.34	+0.78	Ni_4O_4	-2.96	+2.18	-2.12	+0.06

Figure captions

Fig. 1 Illustration of bulk β-Ga_2O_3 crystal and stoichiometric surfaces: (a) bulk, (b) (100)-A, (c) (100)-B, (d) (001)-A, (e) (001)-B, (f) (010). The red and brown balls stand for oxygen and gallium, respectively.

Fig. 2 Surface energies (in J/m^2) of fully optimized (100)-A, (100)-B, (001)-A, (001)-B and (010) surfaces of β-Ga_2O_3 as a function of the number *n* of stoichiometric repeated layers.

Fig. 3 Density of states for the (100)-B surface of β-Ga_2O_3 calculated by HSE06. The Fermi level is shown through the vertical dashed line.

Fig. 4 Stable configurations of $Ni_n/Ga_2O_3(100)$ (n=1-4) clusters (side and top views). Relative energies with respect to the corresponding lowest-energy structure are shown. Coloring scheme: red (surface O), brown (Ga) and blue (Ni). This color scheme applies to the following figure.

Fig. 5 Geometrical parameters for the most stable structures of $Ni_n/Ga_2O_3(100)$ (n=1-4): (a) Ni, (b) Ni_2, (c) Ni_3, and (d) Ni_4.

Fig. 6 Density of states for the most stable configuration of (a) Ni, (b) Ni_2, (c) Ni_3, and (d) Ni_4 adsorbed on $Ga_2O_3(100)$ surface. The Fermi level is shown by the vertical dashed line.

Fig. 7 Stable configurations of $Ni_nO_n/Ga_2O_3(100)$ (n=1-4) clusters (side and top views). Relative energies with respect to the corresponding lowest-energy structure are shown. Coloring scheme: red (surface O), brown (Ga), yellow (adsorbed O) and blue (Ni). The same color scheme applies to all the following figures.

Fig. 8 Geometrical parameters for the most stable structures of $Ni_nO_n/Ga_2O_3(100)$ (n=1-4): (a) Ni, (b) Ni_2, (c) Ni_3, and (d) Ni_4.

Fig. 9 Density of states for the most stable configuration of (a) NiO, (b) Ni_2O_2, (c) Ni_3O_3 and (d) Ni_4O_4 adsorbed on $Ga_2O_3(100)$ surface. The Fermi level is shown by the vertical dashed line.

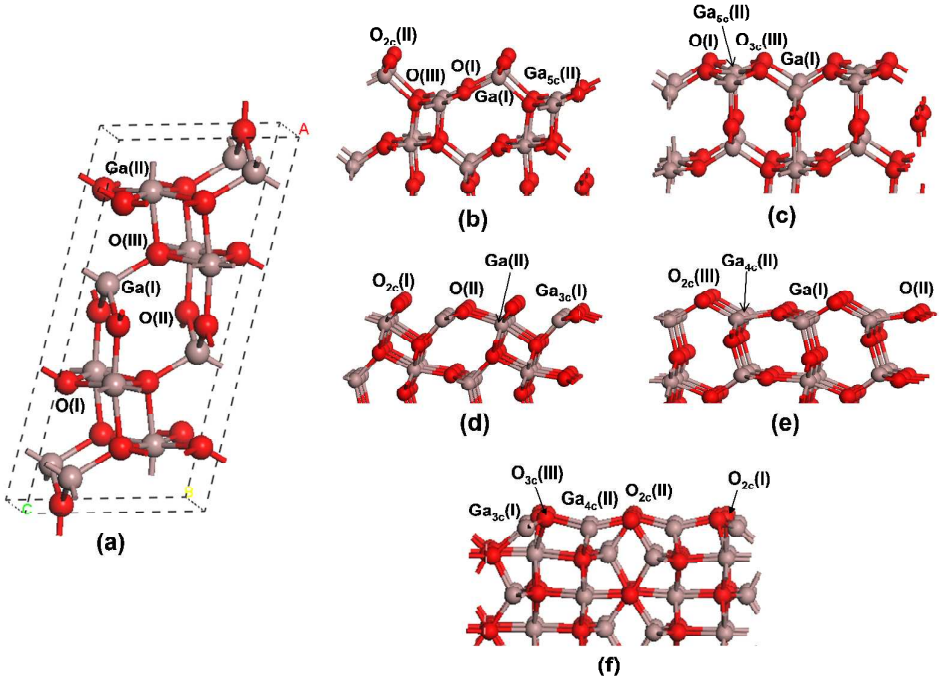

Fig. 1

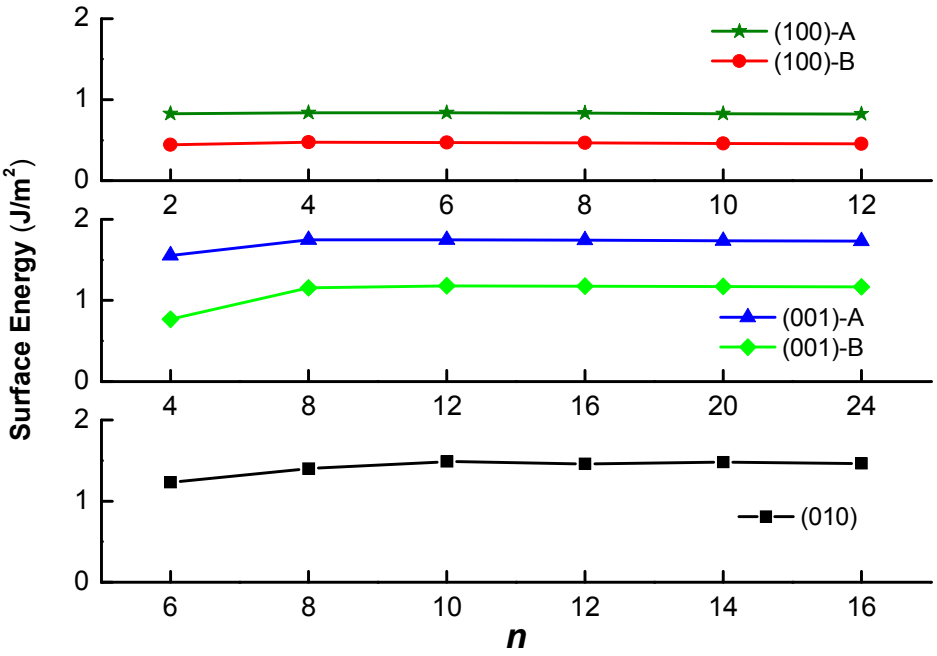

Fig. 2

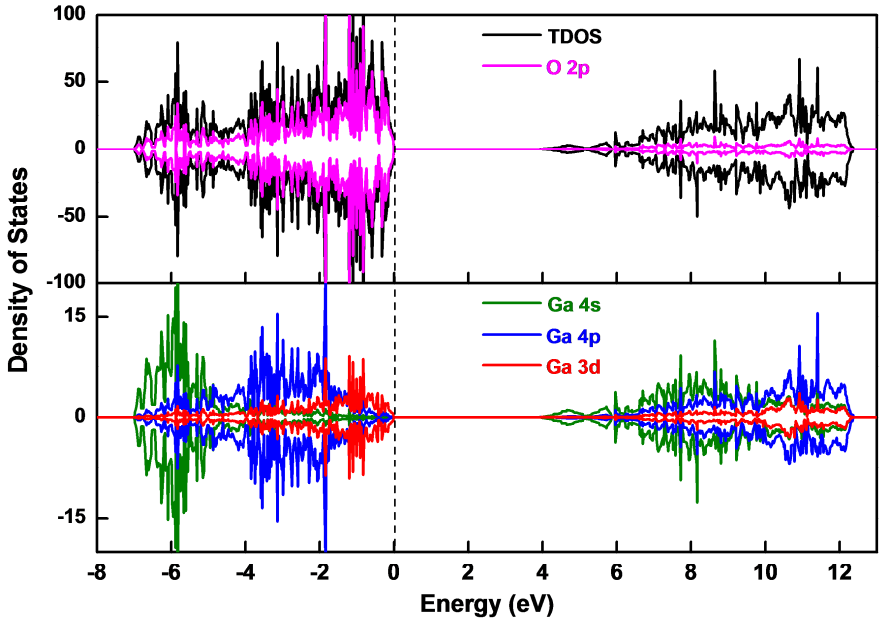

Fig. 3

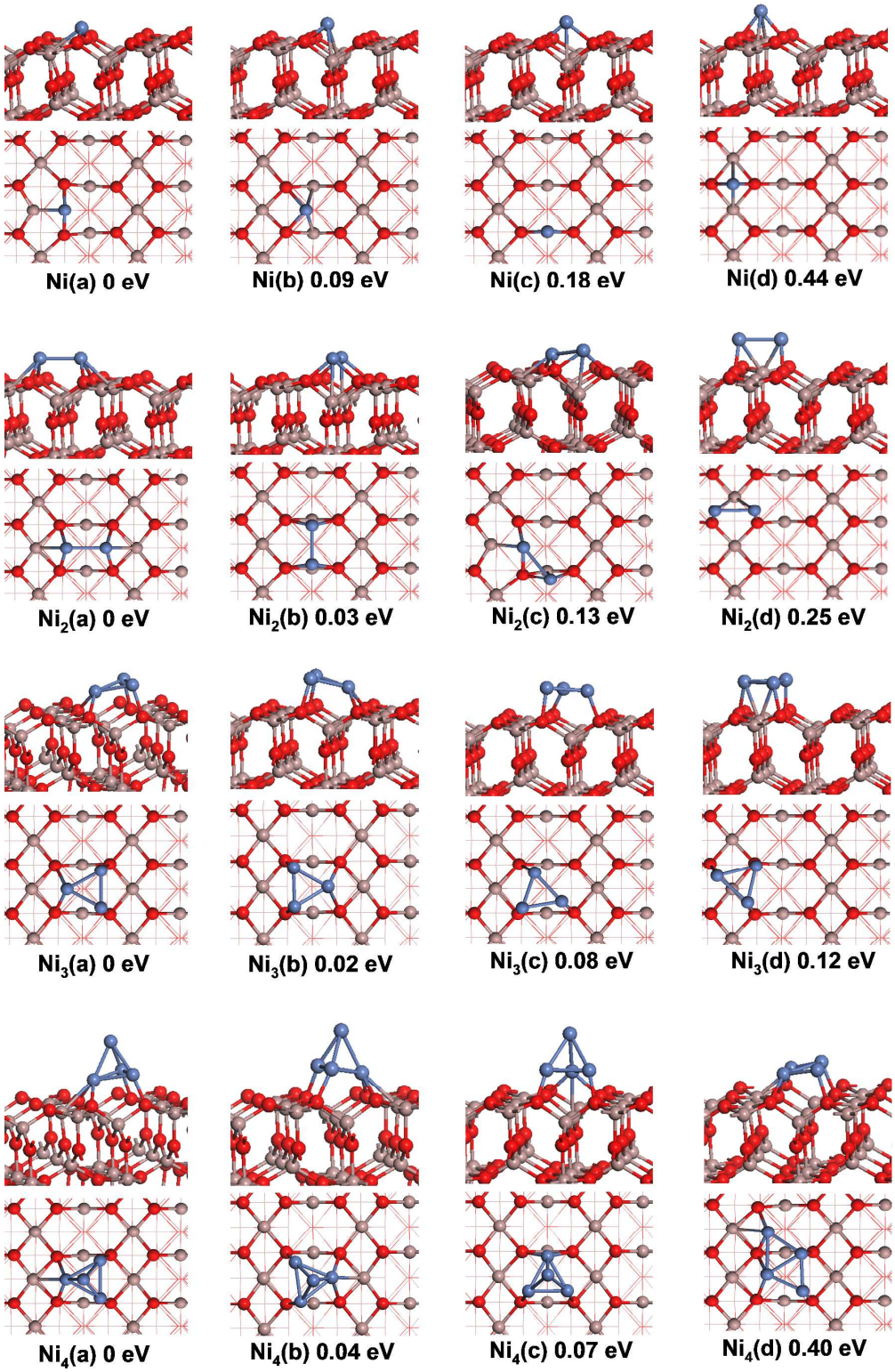

Fig. 4

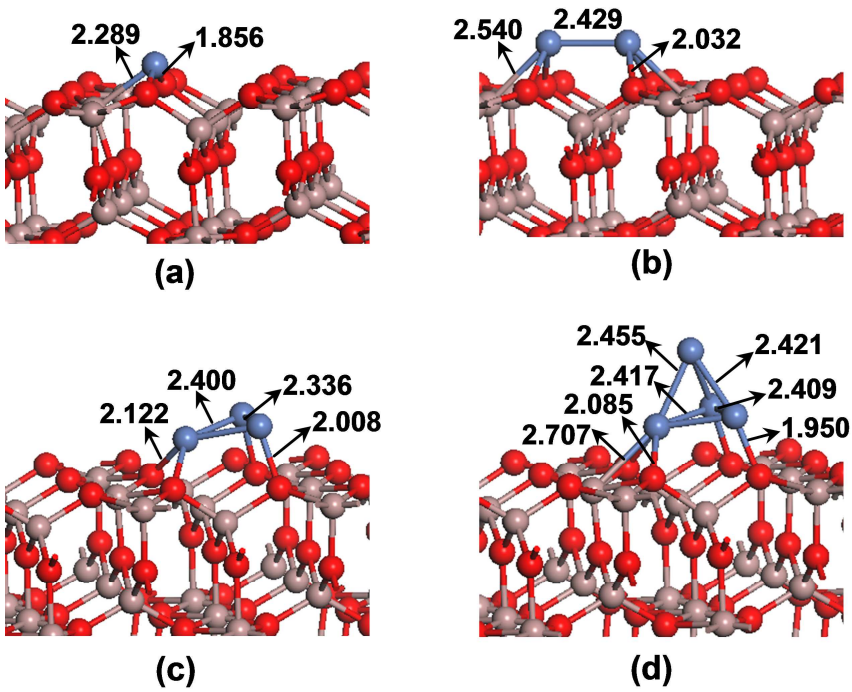

Fig. 5

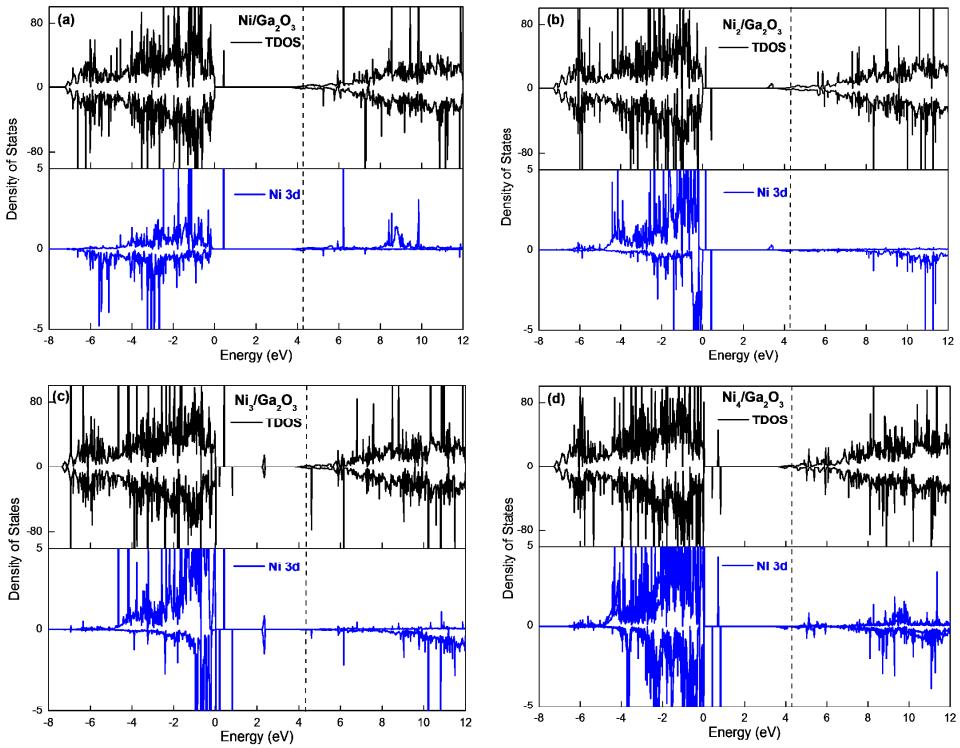

Fig. 6

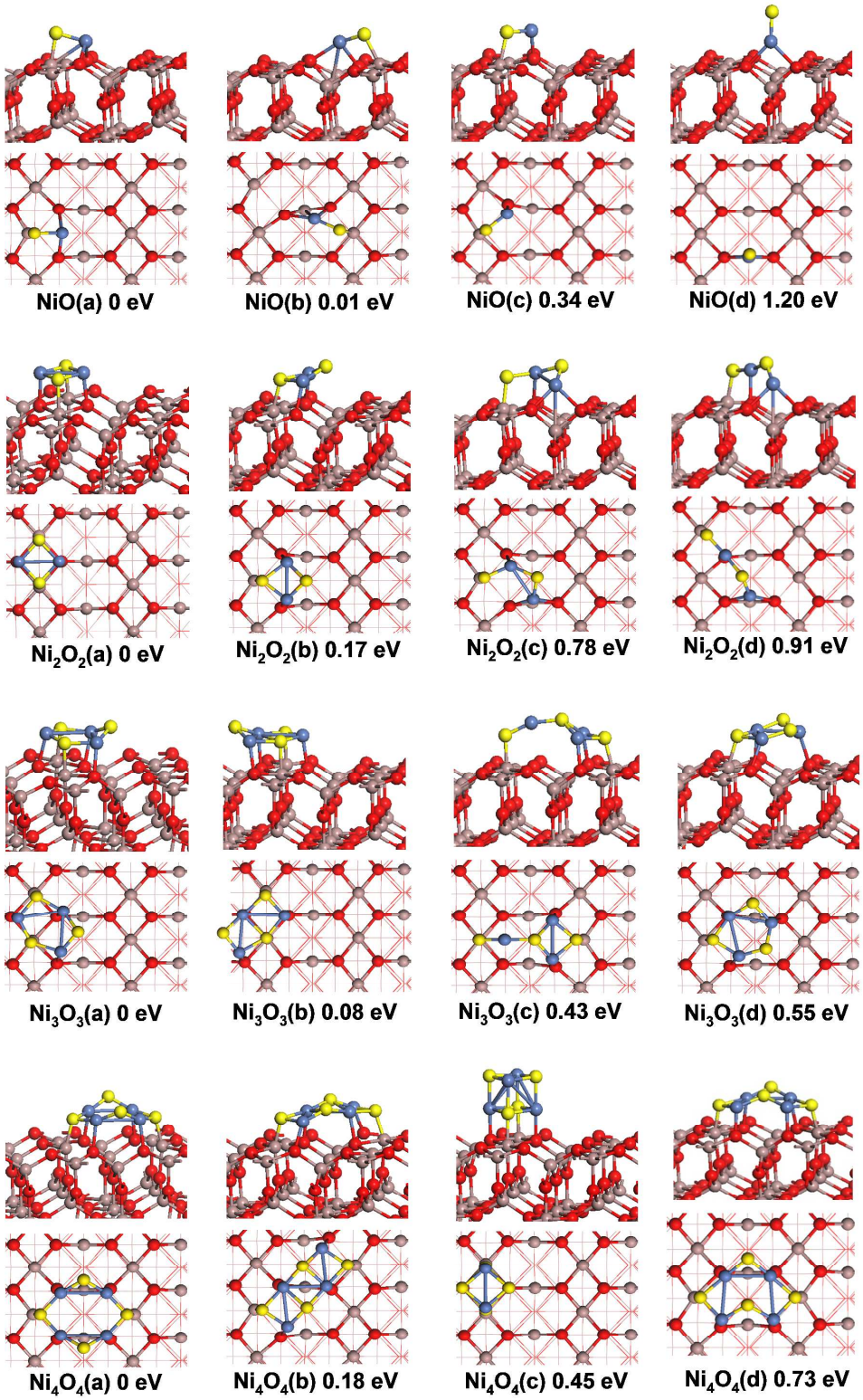

Fig. 7

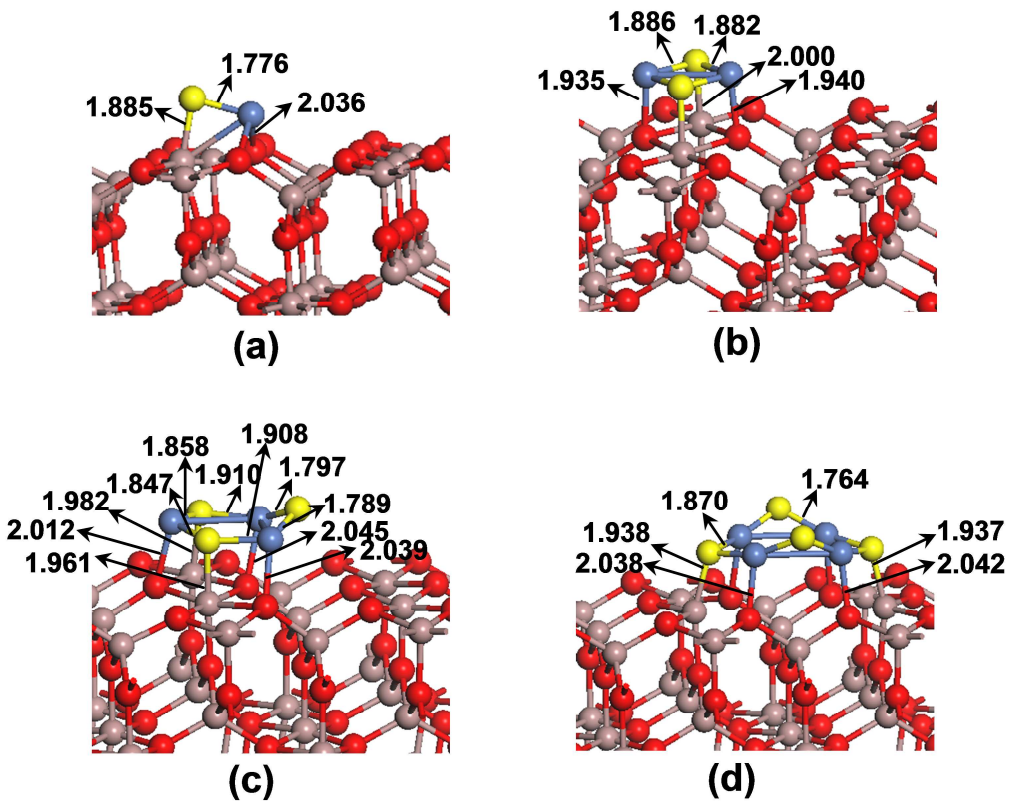

Fig. 8

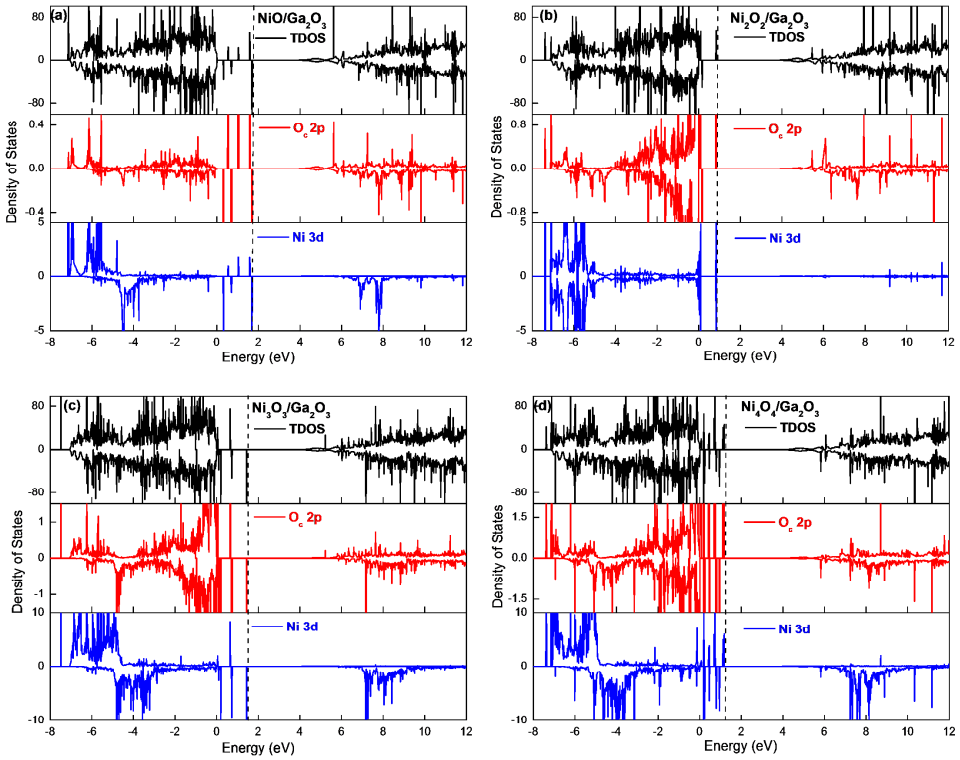

Fig. 9